

ARTICLE

Open Access

Phase-change-driven dielectric-plasmonic transitions in chalcogenide metasurfaces

Behrad Gholipour^{1,2}, Artemios Karvounis¹, Jun Yin³, Cesare Soci³, Kevin F. MacDonald¹ and Nikolay I. Zheludev^{1,3}

Abstract

Chalcogenides—alloys based on group-16 ‘chalcogen’ elements (sulfur, selenium, and tellurium) covalently bound to ‘network formers’ such as arsenic, germanium, antimony, and gallium—have a variety of technologically useful properties, including infrared transparency, high optical nonlinearity, photorefractivity and readily induced, reversible, non-volatile structural phase switching. Such phase-change materials are of enormous interest in the fields of plasmonics and nanophotonics. However, in such applications, the fact that some chalcogenides accrue plasmonic properties in the transition from an amorphous to a crystalline state, i.e., the real part of their relative permittivity becomes negative, has gone somewhat unnoticed. Indeed, one of the most commercially important chalcogenide compounds, germanium antimony telluride ($\text{Ge}_2\text{Sb}_2\text{Te}_5$ or GST), which is widely used in rewritable optical and electronic data storage technologies, presents this behavior at wavelengths in the near-ultraviolet to visible spectral range. In this work, we show that the phase transition-induced emergence of plasmonic properties in the crystalline state can markedly change the optical properties of sub-wavelength-thickness, nanostructured GST films, allowing for the realization of non-volatile, reconfigurable (e.g., color-tunable) chalcogenide metasurfaces operating at visible frequencies and creating opportunities for developments in non-volatile optical memory, solid state displays and all-optical switching devices.

Introduction

Phase-change materials have had a significant role in the evolution of active plasmonic and photonic metamaterial technologies, delivering a variety of switchable, tunable, and reconfigurable optical functionalities through hybridization with plasmonic metal nanostructures^{1–5}. Chalcogenides, which can be electrically and optically switched between amorphous and crystalline states with markedly different electronic and photonic properties^{6–10}, have facilitated the realization of active plasmonic metamaterial devices for a variety of applications including electro- and all-optical signal switching, polarization modulation, beam steering, and

multispectral imaging^{11–19}. Moreover, the near-infrared high refractive index and index contrast between phase states within germanium antimony telluride ($\text{Ge}_2\text{Sb}_2\text{Te}_5$ or GST) have recently been harnessed in the demonstration of laser-rewritable and optically switchable, nanostructured ‘all-dielectric’ (i.e., all-chalcogenide) metasurfaces^{20–22}. At the same time, several bulk monocrystalline chalcogenides have been recognized as ‘topological insulators’ (TIs)—semiconductors with topologically protected metallic surface states arising through strong spin–orbit interactions²³. Indeed, the quaternary TI alloy $\text{Bi}_{1.5}\text{Sb}_{0.5}\text{Te}_{1.8}\text{Se}_{1.2}$ (BSTS) has recently been demonstrated as a UV–visible range plasmonic medium²⁵.

Here, we show that thin-film GST can be optically switched between amorphous and polycrystalline states, which are dielectric and metallic (i.e., plasmonic) respectively at UV/VIS wavelengths, and demonstrate this switching in the context of photonic metasurfaces.

Correspondence: Behrad Gholipour (b.gholipour@soton.ac.uk) or Kevin F. MacDonald (kfm@orc.soton.ac.uk)

¹Optoelectronics Research Centre & Centre for Photonic Metamaterials, University of Southampton, Highfield, Southampton, SO17 1BJ, UK

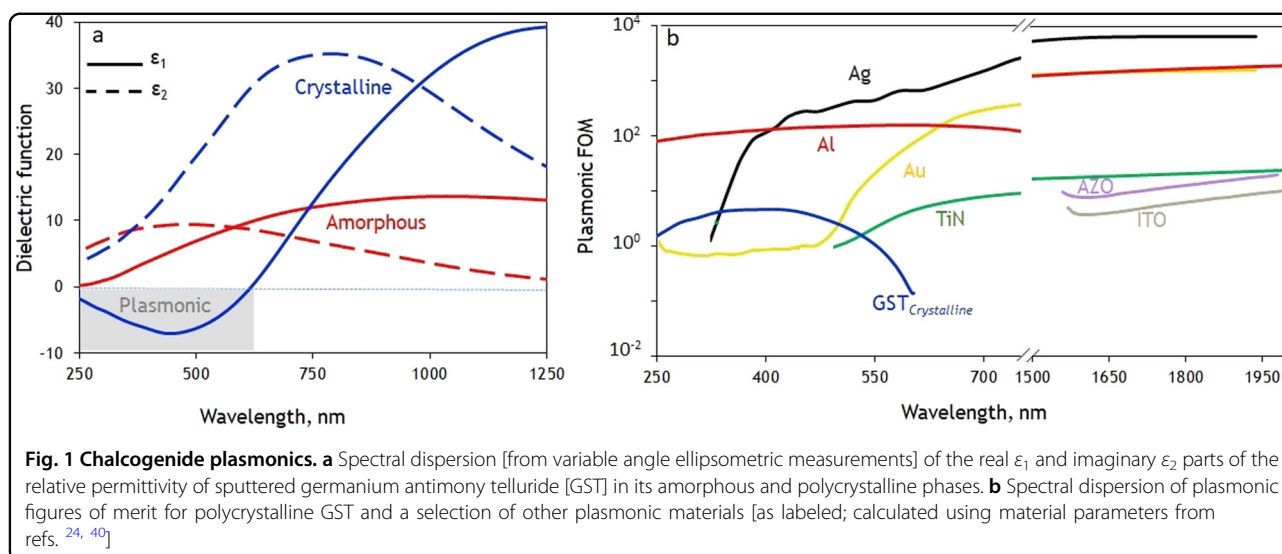
²School of Chemistry, University of Southampton, Highfield, Southampton, SO17 1BJ, UK

Full list of author information is available at the end of the article

© The Author(s) 2018



Open Access This article is licensed under a Creative Commons Attribution 4.0 International License, which permits use, sharing, adaptation, distribution and reproduction in any medium or format, as long as you give appropriate credit to the original author(s) and the source, provide a link to the Creative Commons license, and indicate if changes were made. The images or other third party material in this article are included in the article's Creative Commons license, unless indicated otherwise in a credit line to the material. If material is not included in the article's Creative Commons license and your intended use is not permitted by statutory regulation or exceeds the permitted use, you will need to obtain permission directly from the copyright holder. To view a copy of this license, visit <http://creativecommons.org/licenses/by/4.0/>.



The real part ϵ_1 of the relative permittivity (Fig. 1a) of polycrystalline GST has a negative value at wavelengths λ below 660 nm, as is required for a medium in air/vacuum to support surface plasmons²⁶, and a positive value at longer wavelengths. In contrast, amorphous GST is dielectric with a positive value of ϵ_1 across the entire ultraviolet to near-infrared spectral range. Figure 1b presents the plasmonic figures of merit $Re\{k_{SPP}\}/2\pi Im\{k_{SPP}\}$ —the surface plasmon polariton (SPP) propagation decay length in units of SPP wavelength²⁷—for polycrystalline GST alongside a number of other, noble metals and recently proposed alternative²⁸ plasmonic media. ($k_{SPP} = k_0 \sqrt{\epsilon_m \epsilon_d / (\epsilon_m + \epsilon_d)}$ is the wavevector of the surface plasmon polaritons on a planar interface between the metallic and dielectric media with complex relative permittivities of ϵ_m and ϵ_d , respectively; the latter is taken to be air in the present case; k_0 is the free space wavevector). On this basis, GST is surpassed only by Al in the near-UV spectral range and is comparable as a plasmonic medium for UV and blue/green visible wavelengths to highly doped transparent conductive oxides at near-infrared wavelengths.

In isolation, optically thick GST is an absorbing medium at ultraviolet/visible wavelengths with a dispersion of reflectivity that can be substantially modified by nano-grating metasurface structures, yielding vibrant plasmonic colors in the crystalline state when illuminated with light polarized perpendicular to the grating lines (see Supplementary Figure S1). For the present study however, we adopt an encapsulated layer structure closer to that which would ultimately be required in a practical reversible switching device, whereby a thin chalcogenide film is protected against atmospheric degradation, especially at elevated phase-transition temperatures¹¹. While this encapsulation does have

the effect of suppressing absolute levels of reflectivity and transmission relative to those of a free-standing thin film (a result of Fabry–Perot-type interference between the central high-index absorbing film and lower-index layers either side²⁹), it nonetheless facilitates a demonstration of an optically induced change in the character of the chalcogenide, from dielectric to plasmonic.

Materials and methods

For the present study, 70 nm of GST was deposited between 70 nm protective layers of ZnS/SiO₂ on an optically flat quartz substrate by RF sputtering (Kurt J. Lesker Nano 38) from Ge₂Sb₂Te₅ and ZnS:SiO₂ (1:9) alloy targets. A base pressure of 5×10^{-7} mbar was achieved prior to the deposition, and high-purity argon was used as the sputtering gas. The substrate was held within 10 K of room temperature on a rotating plate 150 mm from the target to produce low-stress amorphous films. The chemical composition of the deposited phase-change film was confirmed using energy dispersive X-ray spectroscopy (Supplementary Figure S2). Nano-grating metasurface arrays were subsequently milled though the ZnS/SiO₂–GST–ZnS/SiO₂ tri-layer using a focused (gallium)-ion beam (FEI Helios NanoLab 600) at beam currents ≤ 28 pA to prevent crystallization of the GST (via ion beam-induced heating) during the milling process. Metasurface domains, each measuring 20×20 μ m in the sample plane, were fabricated with a range of periods, P , from 250 to 400 nm at a fixed milled line-width, W , of 100 nm (Fig. 2).

The amorphous-to-crystalline transition in chalcogenides is an annealing process that may be initiated across the whole sample by increasing the ambient temperature or locally by laser- or electrical current-induced heating to a temperature above the material's

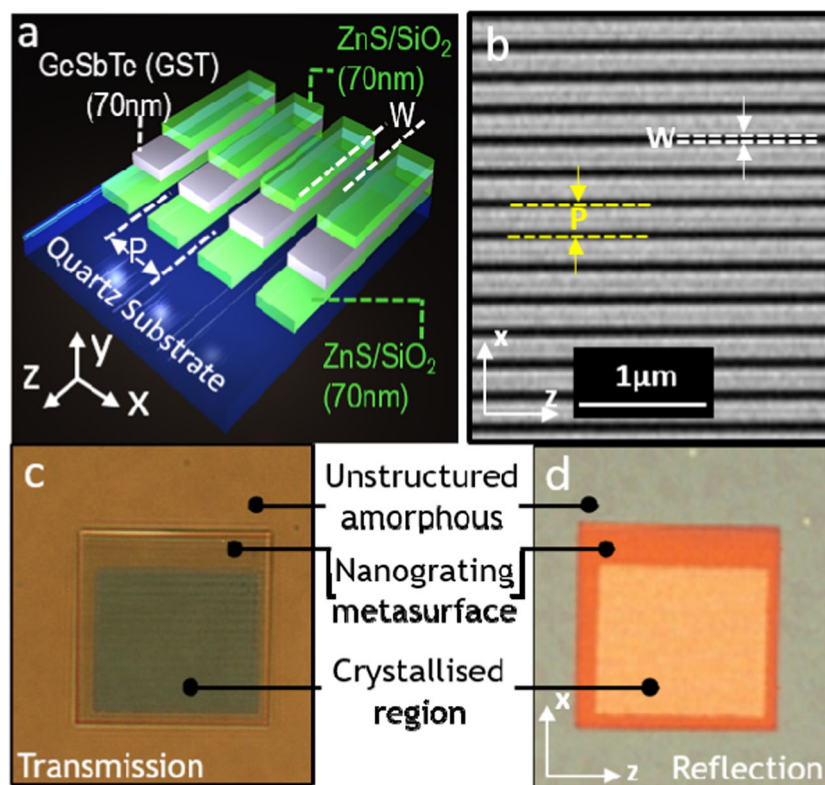


Fig. 2 GST metasurfaces. **a** Artistic cut-away section of the nanograting metasurface structures fabricated with a 70 nm film of GST between two layers [70 nm each] of ZnS/SiO₂. **b** Scanning electron microscopy image of a section of a ZnS/SiO₂–GST–ZnS/SiO₂ tri-layer metasurface [dark areas are the quartz substrate exposed by focused ion-beam milling, i.e., removal of the tri-layer]. **c** Transmission and **d** reflection TM-polarized, normal-incidence reflection images of a 20 × 20 μm, $P = 400$ nm, amorphous phase, GST, tri-layer metasurface domain [surrounded by unstructured, amorphous phase GST tri-layer], part of which—the central 12 × 12 μm region appearing green in transmission mode and pale orange in reflection mode—has been selectively crystallized by fs-pulsed laser illumination

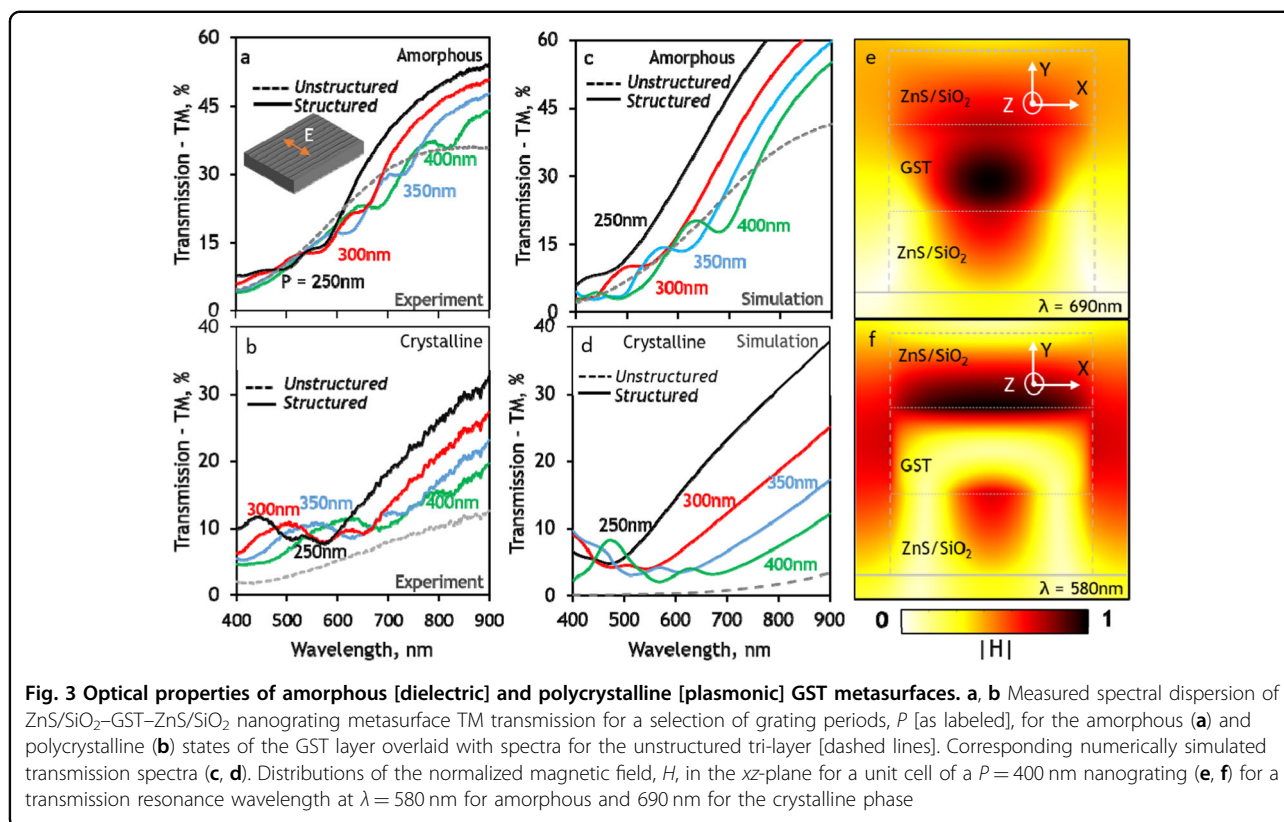
glass-transition point, T_g ($\sim 160^\circ\text{C}$ for GST), but below its melting point, T_m ($\sim 600^\circ\text{C}$)³⁰. The reverse transition—a melt-quenching process—can be driven by shorter, higher energy pulsed excitation that momentarily brings the material to a temperature above T_m ³¹. In this work, structural transitions in the GST layer were excited using 85 fs laser pulses at a wavelength of 730 nm with a beam focused to a diffraction-limited spot and raster-scanned over the sample using a spatial light modulator, as described in ref. ³² By varying the number, repetition rate and energy of the pulses delivered at a given point, one may accurately control the temporal profile of the optically induced temperature change in the GST. Here, we employed trains of fifty $\sim 140\text{ mJ cm}^{-2}$ pulses at a repetition rate of 1 MHz for crystallization.

The normal-incidence transmission and reflection characteristics of the GST nanograting metasurfaces in amorphous and crystalline states were quantified for incident polarizations perpendicular and parallel to the grating lines (along the x and z directions defined in Fig. 2 or the TE and TM orientations of the grating,

respectively) using a microspectrophotometer (CRAIC QDI2010) with a sampling domain size of $15\text{ }\mu\text{m} \times 15\text{ }\mu\text{m}$ and numerical aperture of 0.28.

Results and discussion

For GST in the amorphous phase, the transmission of the unstructured ZnS/SiO₂–GST–ZnS/SiO₂ tri-layer increases monotonically with the wavelength across the UV-to-near-IR spectral range, from $\sim 5\%$ at 400 nm to 35% at 900 nm (Fig. 3a). For the polycrystalline phase, transmission levels are suppressed across the entire range but follow essentially the same trend, reaching $\sim 12\%$ at 900 nm (Fig. 3b). The sub-wavelength period (i.e., non-diffractive) nanograting metasurface structures introduce resonances for TM-polarized light (incident electric field perpendicular to the grating lines) at visible wavelengths depending on the period, P , for both phase states of GST, which manifest themselves in the transmitted and reflected colors of the metamaterial domains (Fig. 2c, d). Owing to the highly anisotropic nature of nanograting resonators the optical response



depends on the polarization of the incident light and the resonant peaks disappear with incident polarization parallel to the grooves of the grating (TE). In this orientation, the nanograting behaves as a medium with a non-dispersive effective refractive index related to that of the ZnS/SiO₂-GST-ZnS/SiO₂ stack and its fill fraction within the grating structure. As such, the observed optical response in either amorphous or polycrystalline GST is largely invariant with the nanograting period and almost identical to that of the unstructured tri-layer transmission spectrum for the corresponding phase state. (Corresponding reflection spectra and TE-polarized spectra are presented in Supplementary Figure S3 and S4, respectively).

It should be noted that the observed TM resonances are markedly different for the two phase states of GST. For the amorphous phase, they are displacement current resonances reliant upon the high refractive index contrast between the dielectric GST and the surrounding media, whereas for the crystalline phase, the resonances are plasmonic, i.e., based upon the opposing signs of ϵ_1 at the interfaces between the GST and surrounding media. Numerical simulations clearly illustrate this difference. Figure 3c–f shows the results of a 3D finite-element Maxwell solver model, which employs ellipsometrically measured values for the

complex permittivity of GST, as presented in Fig. 1a. This model assumes lossless non-dispersive refractive indices of 1.46 and 1.80 for the semi-infinite quartz substrate and the ZnS/SiO₂ layers, respectively, normal incident narrowband plane-wave illumination, and due to the periodic boundary conditions, a nanograting pattern of infinite extent in the x - z plane. There is good qualitative and quantitative agreement between the experimentally measured (Fig. 3a, b) and numerically simulated (Fig. 3c, d) transmission spectra for the GST metasurfaces in both amorphous and crystalline states. Discrepancies can be attributed to manufacturing imperfections (the computational model assumes an ideal, rectilinear nanograting geometry, as illustrated schematically in Fig. 2a) and contamination of the ZnS/SiO₂ and GST layers (gallium-ion implantation) during FIB milling, which slightly modifies the refractive index. The cross-sectional distributions of the magnetic field in Fig. 3e and f reveal the essential differences between the resonant modes for the amorphous and crystalline phase of GST. In the former case, the field is stronger within the GST layer (higher index dielectric) than the ZnS/SiO₂ layers above and below, while in the latter, the field is ‘expelled’ from the body of the metallic GST layer and is stronger at the interfaces with ZnS/SiO₂.

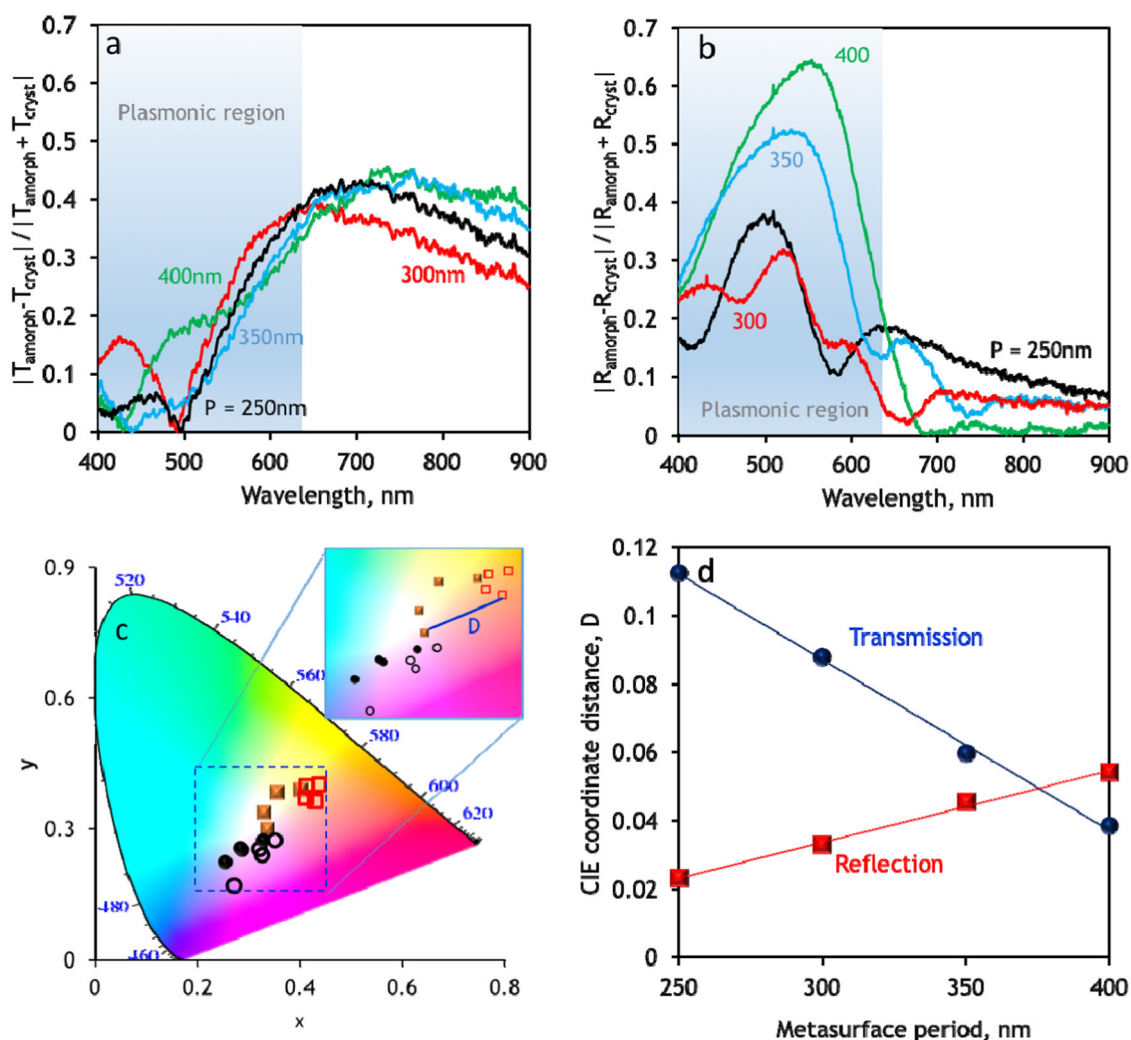


Fig. 4 Switching contrast and color change. Relative **a** transmission and **b** reflection changes induced by the structural change between the amorphous and crystalline phases of the GST metasurfaces with different periods (as labeled). **c** Corresponding reflection (circles) and transmission (squares) CIE color palettes with the marked points indicating the metasurfaces ($P = 250\text{--}400$ nm) shown for both the amorphous (unfilled) and crystalline (filled) phases. **d** Color change resulting from the phase transition quantified as the Euclidean distance [D] in the CIE color plot between corresponding amorphous and crystalline points, given as a function of the metamaterial period

Non-volatile, light-induced structural transitions between the amorphous and crystalline phases of GST, i.e., conversion between dielectric and plasmonic states, change the transmission and reflection characteristics of the metamaterial, which are manifested in the visible spectral range as changes in color. We define the transmission and reflection switching contrast as a ratio of the difference between the levels of the amorphous and crystalline phases of the GST layer to the sum of the levels (Fig. 4a, b). In the present case, the greatest contrast is achieved in reflection at grating period-dependent wavelengths in the spectral band where GST is converted between dielectric and plasmonic forms. The associated changes in color are not though a

straightforward function of (resonant) contrast, they relate to changes in the dispersion of reflectivity and transmission integrated over the entire visible range, and can be quantified within the CIE 1931 color space. The color coordinates for the GST tri-layer metasurfaces in their amorphous and crystalline phases were derived directly from the reflection and transmission spectra (using Judd-Vos-modified CIE 2-deg color matching functions³³ assuming in all cases an illuminating light source with a spectral radiant power distribution of a 6500K black body and normalized observational brightness level) and are plotted in a two-dimensional representation of the CIE 1931 space in Fig. 4c. The change in color brought about by the

structural transition in GST can be quantified as the Euclidean distance between the corresponding points in the CIE space (Fig. 4d) and is remarkably found to be a linear function of the metasurface period, P , for both transmission and reflection. The magnitude of the color change, in these terms, increases with period for reflection and decreases with period for transmission. From a physical point of view, this may be understood to result from a combination of the fact that as the period of the metasurface increases, both reflection and transmission resonances red-shift with a diminishing resonance quality-factor (Q) and that the amorphous to crystalline phase transition broadly increases reflection and decreases transmission. So in reflection, while resonance Q decreases with increasing period, against the background of increasing reflectivity upon crystallization, the magnitude of CIE coordinate change with structural phase increases. Conversely, in transmission, decreasing Q with increasing period, in tandem with a decrease in transmission upon crystallization, results in a decrease in the magnitude of change in CIE coordinate.

In summary, we have shown that switching of the chalcogenide phase-change medium GST between its amorphous and crystalline phases delivers a non-volatile change between dielectric (positive real part of the relative permittivity ϵ) and metallic (negative real part of ϵ) character in the UV–visible spectral range. This behavior enables switching between all-dielectric and plasmonic resonances in nanostructured GST in a sub-wavelength, optically switchable device geometry providing non-volatile changes in transmitted and reflected color. Phase-change chalcogenides have been proposed as potential candidates for future solid-state displays. To obtain the color gamut required, research in this direction has often focused on multilayer (nano)structures in which colour is a designed function of chalcogenide and/or spacer layer thicknesses^{34–37}. On the other hand, the color variations presented by nanograting metasurfaces are achieved with a fixed layer thickness via in-plane structural design at the sub-wavelength scale. Patterns may be engineered to be dependent or independent of the polarization of incident light based (e.g., in the latter case through use of square pillars or circular nanodisk designs). This nanostructural approach can also be used in conjunction with thin-film interference effects, and when optimized through selection of appropriate layer thicknesses can deliver absorptive, transmissive or reflective devices³⁸.

For the purpose of this proof-of-principle demonstration, we chose a commonly used GST composition ($\text{Ge}_2\text{Sb}_2\text{Te}_5$); however, it should be noted that among potential material platforms for photonic metamaterials GST, and more broadly the chalcogenides, offer unique compositional variety (i.e., range and variability of material

parameters) upon changes in stoichiometry, offering the possibility of improved losses and changes in the index with a change in the composition³⁹. Furthermore, they are capable of providing high-index dielectric, ‘epsilon-near-zero’ (ENZ) or topological insulator properties when the constituent elements are combined in the right proportion.

The parameter space for the metasurface design is large, and different structural designs can extend the accessible color range beyond those demonstrated here, giving several extra degrees of freedom in the design of phase-change color pixels. Furthermore, such metasurfaces can be produced over large areas using techniques such as nanoimprint lithography, micro-contact printing or nano-embossing. These scalable manufacturing alternatives to ion-beam milling and reactive etching techniques will also minimize process-related degradation and contamination in the active phase-change layer.

Consequently, such color-tunable metasurfaces offer a robust CMOS (complementary metal–oxide–semiconductor) process compatible material platform for active and reconfigurable metadevices that may find application in thin solid-state displays, data storage, switchable/tunable filters, beam shapers, and optical limiting components.

Data availability

Following a period of embargo, the data from this paper can be obtained from the University of Southampton ePrints research repository: <https://doi.org/10.5258/SOTON/D0449>.

Acknowledgements

The work is supported by the UK Engineering and Physical Sciences Research Council [Grants EP/M009122/1 and EP/N00762X/1] and the Ministry of Education, Singapore [Grants MOE2011-T3-1-005 and MOE2016-T3-1-006].

Author details

¹Optoelectronics Research Centre & Centre for Photonic Metamaterials, University of Southampton, Highfield, Southampton, SO17 1BJ, UK. ²School of Chemistry, University of Southampton, Highfield, Southampton, SO17 1BJ, UK. ³Centre for Disruptive Photonic Technologies, TPI & SPMS, Nanyang Technological University, 21 Nanyang Link, Singapore, 637371, Singapore

Authors' contributions

B.G. generated the idea and designed, and carried out the experiments. A.K. performed the modeling. C.S. and J.Y. performed the DFT modeling. All authors contributed to the interpretation of the results. B.G., N.I.Z., and K.F.M. wrote the manuscript. N.I.Z. supervised the work.

Conflict of interest

The authors declare that they have no conflict of interest.

Publisher's note

Springer Nature remains neutral with regard to jurisdictional claims in published maps and institutional affiliations.

Supplementary information is available for this paper at <https://doi.org/10.1038/s41427-018-0043-4>.

Received: 20 October 2017 Revised: 9 February 2018 Accepted: 5 March 2018

Published online: 11 June 2018

References

- MacDonald, K. F., Krasavin, A. V. & Zheludev, N. I. Optical modulation of surface plasmon-polariton coupling in a gallium/aluminium composite. *Opt. Commun.* **278**, 207–210 (2007).
- Driscoll et al. Memory metamaterials. *Science* **325**, 1176580 (2009).
- Dicken, M. J. et al. Frequency tunable near-infrared metamaterials based on VO₂ phase transition. *Opt. Express* **17**, 18330 (2009).
- Sámson, Z. L. et al. Metamaterial electro-optic switch of nanoscale thickness. *Appl. Phys. Lett.* **96**, 143105 (2010).
- Ahmadivand, A., Gerislioglu, B., Sinha, R., Karabiyik, M. & Pala, N. Optical switching using transition from dipolar to charge transfer plasmon modes in Ge₂Sb₂Te₅ bridged metalodielectric dimers. *Sci. Rep.* **7**, 42807 (2017).
- Shportko, K. et al. Resonant bonding in crystalline phase-change materials. *Nat. Mater.* **7**, 653–658 (2008).
- Lee, T. H. & Elliott, S. R. The relation between chemical bonding and ultrafast crystal growth. *Adv. Mater.* **29**, 1700814 (2017).
- Borisenko, K. B. et al. Photo-induced optical activity in phase-change memory materials. *Sci. Rep.* **5**, 8770 (2015).
- Gholipour, B., Huang, C.-C., Ou, J.-Y. & Hewak, D. W. Germanium antimony lateral nanowire phase change memory by chemical vapor deposition. *Phys. Status Solidi* **250**, 994–998 (2013).
- Hewak, D. & Gholipour, B. Primed to remember. *Science* **336**, 1515–1516 (2012).
- Gholipour, B., Zhang, J., MacDonald, K. F., Hewak, D. W. & Zheludev, N. I. An all-optical, non-volatile, bidirectional, phase-change meta-switch. *Adv. Mater.* **25**, 3050–3054 (2013).
- Michel, A.-K. U. et al. Using low-loss phase-change materials for mid-infrared antenna resonance tuning. *Nano Lett.* **13**, 3470–3475 (2013).
- Chen, Y. G. et al. Hybrid phase-change plasmonic crystals for active tuning of lattice resonances. *Opt. Express* **21**, 13691 (2013).
- Tittel, A. et al. A switchable mid-infrared plasmonic perfect absorber with multispectral thermal imaging capability. *Adv. Mater.* **27**, 4597–4603 (2015).
- Rude, M. et al. Optical switching at 1.55 μm in silicon racetrack resonators using phase change materials. *Appl. Phys. Lett.* **103**, 141119 (2013).
- Cao, T., Zheng, G., Wang, S. & Wei, C. Ultrafast beam steering using gradient Au-Ge₂Sb₂Te₅-Au plasmonic resonators. *Opt. Express* **23**, 18029 (2015).
- Cao, T., Zhang, L., Simpson, R. E. & Cryan, M. J. Mid-infrared tunable polarization-independent perfect absorber using a phase-change metamaterial. *J. Opt. Soc. Am. B* **30**, 1580 (2013).
- Wuttig, M., Bhaskaran, H. & Taubner, T. Phase-change materials for non-volatile photonic applications. *Nat. Photonics* **11**, 465–476 (2017).
- Raeis-Hosseini, N. & Rho, J. Metasurfaces based on phase-change material as a reconfigurable platform for multifunctional devices. *Materials* **10**, 1046 (2017).
- Wang, Q. et al. Optically reconfigurable metasurfaces and photonic devices based on phase change materials. *Nat. Photonics* **10**, 60–65 (2015).
- Karvounis, A., Gholipour, B., MacDonald, K. F. & Zheludev, N. I. directionAll-dielectric phase-change reconfigurable metasurface. *Appl. Phys. Lett.* **109**, 051103 (2016).
- Chu, C. H. et al. Active dielectric metasurface based on phase-change medium. *Laser Photonics Rev.* **10**, 986–994 (2016).
- Zhang, H. et al. Topological insulators in Bi₂Se₃, Bi₂Te₃ and Sb₂Te₃ with a single Dirac cone on the surface. *Nat. Phys.* **5**, 438–442 (2009).
- Werner, W. S. M., Glantschnig, K. & Ambrosch-Draxl, C. Optical constants and inelastic electron-scattering data for 17 elemental metals. *J. Phys. Chem. Ref. Data* **38**, 1013–1092 (2009).
- Yin, J. et al. Plasmonics of topological insulators at optical frequencies. *NPG Asia Mater.* **9**, e425 (2017).
- Barnes, W. L., Dereux, A. & Ebbesen, T. W. Surface plasmon subwavelength optics. *Nature* **424**, 824–830 (2003).
- Dastmalchi, B., Tassin, P., Koschny, T. & Soukoulis, C. M. A new perspective on plasmonics: confinement and propagation length of surface plasmons for different materials and geometries. *Adv. Opt. Mater.* **4**, 177–184 (2015).
- Naik, G. V., Shalae, V. M. & Boltasseva, A. Alternative plasmonic materials: beyond gold and silver. *Adv. Mater.* **25**, 3264–3294 (2013).
- Kats, M. A., Blanchard, R., Genevet, P. & Capasso, F. Nanometre optical coatings based on strong interference effects in highly absorbing media. *Nat. Mater.* **12**, 20–24 (2012).
- Orava, J., Greer, A. L., Gholipour, B., Hewak, D. W. & Smith, C. E. Characterization of supercooled liquid Ge₂Sb₂Te₅ and its crystallization by ultrafast-heating calorimetry. *Nat. Mater.* **11**, 279–283 (2012).
- Liu, Y., Aziz, M. M., Shalini, A., Wright, C. D. & Hicken, R. J. Crystallization of Ge₂Sb₂Te₅ films by amplified femtosecond optical pulses. *J. Appl. Phys.* **112**, 123526 (2012).
- Wang, Q. et al. 1.7 Gbit/in² gray-scale continuous-phase-change femtosecond image storage. *Appl. Phys. Lett.* **104**, 121105 (2014).
- Vos, J. J. Colorimetric and photometric properties of a 2° fundamental observer. *Color Res. Appl.* **3**, 125–128 (1978).
- Hosseini, P., Wright, C. D. & Bhaskaran, H. An optoelectronic framework enabled by low-dimensional phase-change films. *Nature* **511**, 206–211 (2014).
- Schlich, F. F., Zalden, P., Lindenberg, A. M. & Spolenak, R. Color switching with enhanced optical contrast in ultrathin phase-change materials and semiconductors induced by femtosecond laser pulses. *ACS Photonics* **2**, 178–182 (2015).
- Dong, W., Qiu, Y., Yang, J., Simpson, R. E. & Cao, T. Wideband absorbers in the visible with ultrathin plasmonic-phase change material nanogratings. *J. Phys. Chem. C* **120**, 12713–12722 (2016).
- Rios, C., Hosseini, P., Taylor, R. A. & Bhaskaran, H. Color depth modulation and resolution in phase-change material nanodisplays. *Adv. Mater.* **28**, 4720–4726 (2016).
- Häggglund, C., Apell, S. P. & Kasemo, B. Maximized optical absorption in ultrathin films and its application to plasmon-based two-dimensional photovoltaics. *Nano Lett.* **10**, 3135–3141 (2010).
- Michel, A.-K. U., Wuttig, M. & Taubner, T. Design parameters for phase-change materials for nanostructure resonance tuning. *Adv. Opt. Mater.* **5**, 1700261 (2017).
- Johnson, P. B. & Christy, R. W. Optical constants of the noble metals. *Phys. Rev. B* **6**, 4370–4379 (1972).